Nuclear Data for Science and Technology (1988 MITO), 287- 289, Copyright © 1988 JAERI.

SCATTERING OF 13 MeV NEUTRONS FROM ^{11}B AND ^{28}Si

Yoshimaro Yamanouti, Masayoshi Sugimoto, Yutaka Furuta and Motoharu Mizumoto

Japan Atomic Energy Research Institute
Tokai, Ibaraki 319-11, Japan

Mikio Hyakutake

Department of Nuclear Engineering, Kyushu University
Hakozaki, Fukuoka 812, Japan

Thamrong Methasiri

Department of Physics, Chulalongkorn University
Bangkok 10500, Thailand

Abstract: Differential cross sections for elastic and inelastic scattering of 13MeV neutrons from ^{11}B and ^{28}Si were measured by using the JAERI tandem accelerator. Scattered neutrons were observed by a time-of-flight spectrometer with an array of four 20cmϕ x 35cm NE213 liquid scintillator detectors. Neutron time-of-flight spectra were taken at scattering angles from 20° to 140° for ^{11}B, and from 15° to 140° for ^{28}Si. Inelastic scattering cross sections of neutrons leading to the $1/2^-$(2.125 MeV), $5/2^-$(4.445 MeV) and $3/2^-$(5.021 MeV) states, and the 2^+(1.779 MeV) and 4^+(4.618 MeV) states, of ^{11}B and ^{28}Si, respectively, were measured simultaneously with the elastic cross sections. The experimental cross sections were analyzed in terms of a spherical optical model potential, DWBA and coupled channel calculations using collective model.

(elastic and inelastic scattering, 13MeV, neutron, ^{11}B, ^{28}Si, tandem accelerator, DWBA, coupled-channel formalism, compound nuclear contribution)

Introduction

A few measurements of the neutron scattering on ^{11}B in the energy range above 10 MeV have been made previously. The data available are at neutron energies of 14.1 MeV/1,2/ and 8-14 MeV/3/. Alder et al have studied the inelastic scattering on the low-lying states of ^{11}B by using the unified model, which considers two amplitudes, one corresponding to a ^{12}C core transition and other to a transition of a hole, and have obtained rather good fits to the experimental data/1/.

In this work differential neutron cross sections for elastic and inelastic scattering on ^{11}B were measured at an incident energy of 13 MeV different from other incident energies in order to study the reaction mechanism for the neutron scattering on light odd nuclei. Particular interest was taken in the collective model DWBA or coupled-channel predictions taking into account the inelastic compound nuclear contribution.

As for ^{28}Si, good fits to the experimental data have been obtained with the positive quadrupole deformation parameter as well as the negative quadrupole deformation parameter in the coupled-channel analyses/4,5,6/. Therefore, the nuclear shape of the ground state deformation of ^{28}Si has not been clearly determined. Differential neutron cross sections for the elastic and inelastic scattering on ^{28}Si were measured at 12.8 MeV, and collective properties of low-lying excited states were examined by the coupled-channel formalism.

Experimental method

The measurements were performed with pulsed beam time-of-flight methods. A pulsed beam of deuterons with a repetition rate of 2 MHz and with a burst duration of about 2 nsec was provided by the JAERI tandem electrostatic accelerator. Neutrons were generated by the $^2H(d,n)^3He$ reaction. The gas target was filled with deuterium gas of 2×10^5 Pa. Cylindrical scattering samples of natural silicon (4cm in diam and 4cm in height) and granular natural boron packed in a cylindrical aluminum can were used.

The neutron detector is a 20cm in diam by 35cm thick NE213 liquid scintillator viewed by RCA 8854 photomultiplier tubes at the front and rear scintillator faces. The neutron detector is similar in principle to the very large detector developed at Ohio University/7/. Neutrons were observed by an array of these four neutron detectors for efficient measurements of scattered neutrons. A 5cm in diam by 1.27cm thick NE213 liquid scintillator detector was used as a neutron flux monitor.

The neutron detectors are placed in a detector shield tank. The shield system consists of a shadow bar, a collimator, a pre-shield and a detector shield tank. The flight path of the time-of-flight spectrometer is 8m. The components of the shield system are mounted on a large turntable which is rotatable around the scattering sample.

Data reduction and experimental results

The experimental yields were calculated by fitting the peaks of interest with line shapes of a basic Gausian function with tailing components of the exponential shape multiplied by the complementary error function/8/.

The efficiency of the neutron detector was determined by measuring the known angular distribution of neutrons from the $^{2}H(d,n)^{3}He$ reaction.

The resulting differential cross sections were corrected for the dead time in the time-to-amplitude converters and ADCs in the data acquisition system and for isotope abundance of natural scattering samples. Corrections for multiple scattering, flux attenuation in the sample, angular spread introduced by the finite size of the gas target were also taken into account. These corrections were made by means of the Monte Carlo method with the code MULT1/9/.

Differential cross sections were determined for the elastic scattering and the inelastic scattering leading to the excited states at 2.125 MeV($1/2^-$), 4.445 MeV($5/2^-$) and 5.021 MeV($3/2^-$), and at 1.779 MeV(2^+) and 4.618 MeV(4^+), of ^{11}B and ^{28}Si, respectively. The differential cross sections were measured over the angular range from 20° to 140° in 10° steps at the incident energy of 13 MeV for ^{11}B, and from 15° to 140° in 5° steps at 12.8 MeV for ^{28}Si. The experimental cross sections are shown in figs.1,2 and 3 together with theoretical predictions.

Analysis

Optical model analysis for ^{11}B

The elastic scattering data for ^{11}B were analyzed by the optical model with the standard form. The optical potential parameters except the spin orbit term were searched for to give the best fit between the calculated cross sections for the shape elastic scattering plus the compound elastic scattering and the measured elastic scattering cross sections.

The compound elastic and inelastic cross sections were estimated by using the Hauser-Feshbach formalism. The (n,n), (n,p), (n,d), (n,t) and (n,α) channels were taken into account for the outgoing channels in the compound nuclear process. For the (n,n') channel the level density formulae/10/ were applied to the excited states higher than 8 MeV. The compound cross sections were scaled down by the reduction coefficient/11/ of 0.58 to correct the overestimate for the calculated values. These calculations were performed by means of the code ELIESE-3/12/. The theoretical cross sections obtained in the optical model analysis are shown in fig. 1.

DWBA calculation for ^{11}B

It is of great interest to study to what extent the collective model can describe the light mass nucleus ^{11}B. Collective model predictions were examined by using the code DWUCK4/13/. In the DWBA calculations the best fit optical potential parameters obtained in the optical model analysis were used. And compound inelastic cross sections were taken into account in the DWBA fits. The result obtained in the DWBA calculation for the $5/2^-$ state is shown in fig. 1.

Coupled-channel calculations for ^{11}B

The experimental cross sections were also analyzed by the coupled-channel(CC) formalism by using the code ECIS79/14/ to check the nuclear shape. In the CC calculations the $3/2^-$ ground state and the $5/2^-$ state at 4.445 MeV were assumed to be the members of the K=3/2 rotational band. Optical potential parameters except the spin orbit term and the deformation parameter β_2 were adjusted to get the best fit to the experimental cross sections. The results obtained in the CC calculations are shown in fig. 2. The fits to the experimental cross sections for the $5/2^-$ state are good. The quality of the fit with oblate deformation is nearly equal to that with prolate deformation.

Coupled-channel calculations for ^{28}Si

The CC calculations based on the rotational model were carried out in order to find whether the nuclear shape of ^{28}Si is oblate or prolate by using the code ECIS79. The 0^+(0.0 MeV), 2^+(1.779 MeV) and 4^+(4.618 MeV) states were treated as the members of the ground state rotational band. The calculations were performed with the 0^+-2^+-4^+ coupling scheme assuming the quadrupole deformation only and the quadrupole and hexadecapole deformation. In the CC calculations optical potential parameters except the spin orbit term and the deformation parameters were adjusted to get the best fits to the experimental cross sections for the elastic and inelastic scattering. The result of the CC calculation with the quadrupole deformation only reproduces the ground and 2^+ cross sections well, whereas the prediction for the 4^+ state is systematically smaller in magnitude than the experimental data in the whole angular range, and does not reproduce the pattern of the angular distribution. It is to be noticed here that each theoretical curve calculated in the DWBA and CC analyses in figs. 1,2 and 3 is the incoherent superposition of the direct contribution and the compound nuclear contribution. The result of the CC calculation for ^{28}Si is represented in fig. 3. And the best fit optical potential parameters and the deformation parameters obtained in the CC calculation are listed in table 1. It is clear in fig. 3 that the CC calculation with the oblate quadrupole deformation and the hexadecapole deformation gives the best fit to the experimental cross sections for the 0^+, 2^+ and 4^+ states.

Conclusions

Acculate measurements of experimental neutron cross sections for elastic and inelastic scattering on ^{11}B and ^{28}Si have been made. The collective model calculations taking into account the compound nuclear contribution well reproduce the experimental cross sections for the $3/2^-$ and $5/2^-$ states of ^{11}B, and result in reasonable values of the deformation parameters reflecting the deformation of the ^{12}C core. The results of the present CC calculations support the oblate quadrupole deformation of ^{28}Si.

The measured cross sections obtained in the present experiment are widely useful for the nuclear data for applications.

References

1. J.C. Alder and B. Vaucher: Nucl. Phys. A147, 657(1970)
2. M.Hyakutake, M. Sonoda, A. Katase, Y. Wakuta M.Matoba, H. Tawara and I. Fujita: J. Nucl. Sci. Technol. 11, 407(1974)
3. S.G. Glendinning et al: Nucl. Sci. Eng. 80, 256(1982)
4. G. Haouat et al: Phys. Rev. C30, 1795(1984)
5. A.G. Blair et al: Phys.Rev. C1, 444(1970)
6. R. De Leo et al: Phys. Rev. C20, 1244(1979)
7. J.D. Carlson et al: Nucl. Instr. 147, 353 (1977)
8. G.W. Phillips et al: Nucl. Instr. 137, 525 (1976)
9. A. Kohsaka and Y. Tomita (unpublished)
10. A. Gilbert et al: Can. J. Phys. 43, 1446(1965)
11. B. Zwieglinski et al: Nucl. Phys. A209, 348 (1973)
12. S. Igarasi: JAERI report, JAERI-1224 (1972)
13. P.D. Kuntz: code DWUCK4, (unpublished)(1976)
14. J. Raynal: code ECIS79 (unpublished)

Table 1. OP and deformation parameters

	^{11}B		^{28}Si
	OP(DWBA)	CC	CC
V_R	47.33	47.36	49.24
r_R	1.296	1.276	1.184
a_R	0.420	0.443	0.739
W_D	8.37	8.19	6.77
r_D	1.186	1.259	1.273
a_D	0.410	0.334	0.524
V_{SO}	5.66	5.66	6.0
r_{SO}	1.27	1.27	1.15
a_{SO}	0.47	0.47	0.58
β_2	0.54	-0.566	-0.397
β_4			0.181

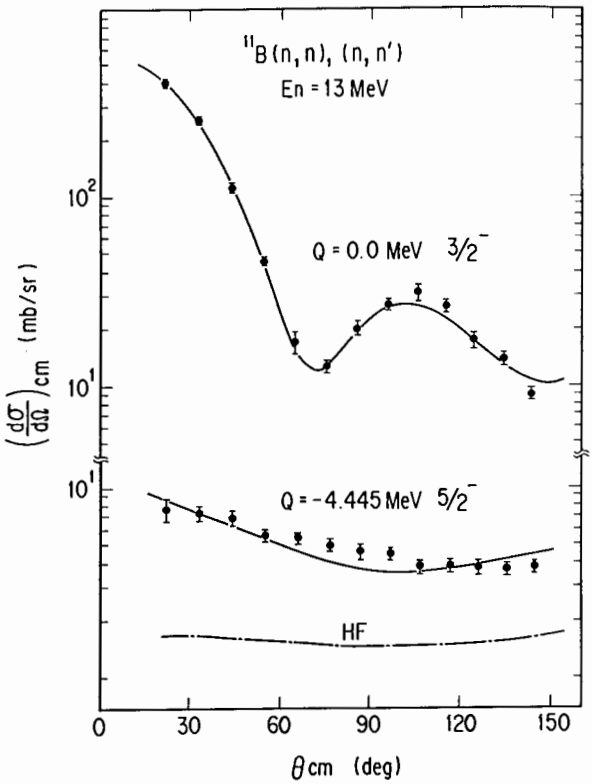

Fig. 1 Experimental cross sections, and DWBA and HF predictions for ^{11}B

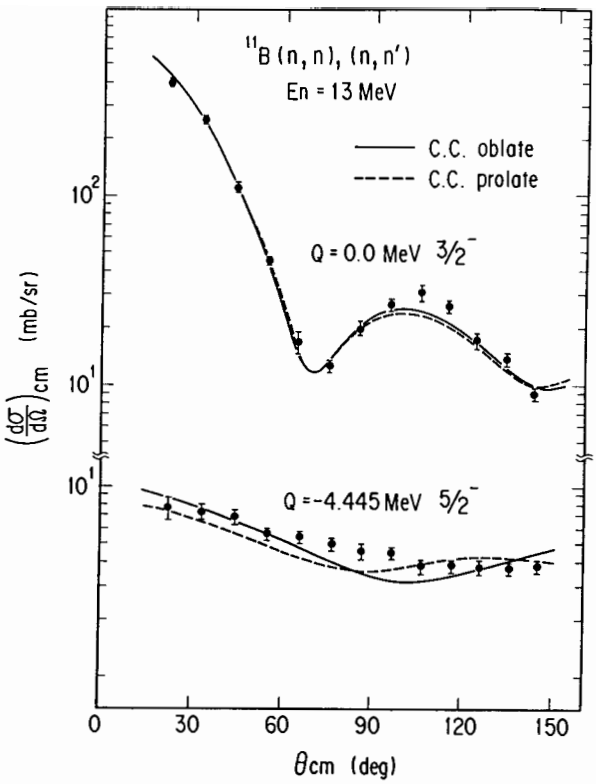

Fig. 2 Experimental cross sections and CC predictions for ^{11}B

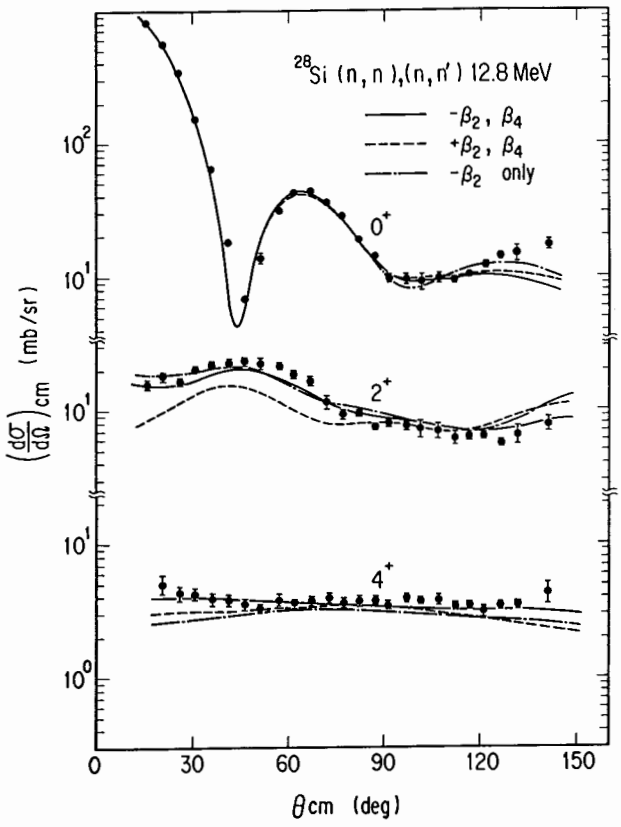

Fig. 3 Experimental cross sections and CC predictions for ^{28}Si